Available online at www.sciencedirect.com
SCIENCE DIRECT®

Journal of the European Ceramic Society 24 (2004) 129–137

www.elsevier.com/locate/jeurceramsoc

Synthesis and characterization of $(La_{1-x}M_x)_2Mo_2O_{9-\delta}$; $M = Ca^{2+}$, Sr^{2+} or Ba^{2+}

R. Subasri, D. Matusch, H. Näfe*, F. Aldinger

Max-Planck-Institut für Metallforschung, Pulvermetallurgisches Laboratorium, Heisenbergstrasse 3, D- 70569, Stuttgart, Germany

Received 15 January 2003; received in revised form 27 February 2003; accepted 7 March 2003

Abstract

The system $(La_{1-x}Ca_x)_2Mo_2O_{9-\delta}$ was characterized in the region $x = 0.01 \leqslant x \leqslant 0.15$ by slow-scan powder X-ray diffraction measurements in order to determine the solubility limit of CaO. For the sake of comparison, the same was repeated for $(La_{1-x}M_x)_2Mo_2O_{9-\delta}$ where $M = Sr^{2+}$ or Ba^{2+} and $x = 0.05$ and 0.10, respectively. In addition, the electrical conductivities of some of the typical compositions investigated in the present study were measured as a function of temperature by means of the ac impedance technique. The suppression of the phase transition in $La_2Mo_2O_9$ by the alkaline-earth dopants was verified by differential thermal analysis of the samples.

Keywords: Functional applications; Impedance; Ionic conductivity; Powders-chemical preparation; Solubility limit; X-ray methods

1. Introduction

There are ongoing efforts in the literature in order to replace the conventional yttria stabilized zirconia (YSZ) by alternate oxide-ion conducting materials for use at lower temperatures. Recently, Lacorre et al. reported a high oxide-ion conductivity in $La_2Mo_2O_9$,[1–3] a material which has been known as early as 1970.[4] This material undergoes a structural phase transition at 853 K from a monoclinic form to a cubic structure. At the transition temperature, the oxide-ion conductivity is reported to increase sharply by nearly two orders of magnitude, reaching values higher than those of YSZ. Aliovalent substitution at either the La^{3+} or Mo^{6+} sites is expected to suppress the phase transition and thus increase the conductivity by increasing the defect concentration. Several dopants were investigated by Lacorre et al., but, no emphasis was laid on doping with Ca^{2+} on the La^{3+} sites.[5] This is all the more surprising as Ca^{2+} is expected on the basis of ionic radius to be a better substitute than the alkaline-earth dopants Sr^{2+} or Ba^{2+} with $r_{Ca2+} = 118$ pm for nine-fold coordination. Ca^{2+} has a similar ionic radius to that of La^{3+} ($r_{La3+} = 121.6$ pm). However, so far, there has been only one report by Wang and Fang on CaO doped $La_2Mo_2O_9$, where it was stated that up to 15 mol% of Ca^{2+} could be conveniently accommodated on the La^{3+} sites.[6] The powder X-ray diffraction (XRD) patterns of the doped samples reported by Wang and Fang showed the presence of additional peaks, which were not accounted for. Due to the attractive applications of the material, especially of the CaO doped one as a solid electrolyte for intermediate temperature applications, an exact knowledge about the limit of solubility of CaO in $La_2Mo_2O_9$ is desirable.

It is the aim of the present investigation to determine this solubility limit by measuring the lattice constant of the solid solutions as a function of the composition and to corroborate the results by other techniques.

2. Experimental

2.1. Synthesis

The synthesis of all materials for this investigation was carried out by a wet chemical process, i.e. a modified Pechini route. Seven compositions of CaO doped

* Corresponding author. Tel.: +49-711-6893113; fax: +49-711-6893131.
E-mail address: naefe@mf.mpg.de (H. Näfe).

0955-2219/03/$ - see front matter © 2003 Elsevier Ltd. All rights reserved.
doi:10.1016/S0955-2219(03)00123-7

$La_2Mo_2O_9$ namely $(La_{1-x}Ca_x)_2Mo_2O_{9-\delta}$ with $x=0.01$, 0.02, 0.03, 0.04, 0.05, 0.1 and 0.15 were prepared. For the sake of comparison, $(La_{1-x}Ca_x)_2Mo_2O_{9-\delta}$ where $M=Sr^{2+}$ and Ba^{2+} with $x=0.05$ and 0.1, respectively, were also synthesized by a similar procedure. The values of x for Sr and Ba doping were reported to be the solubility limits for those cations.[5] $La(NO_3)_3.6H_2O$, $Ca(NO_3)_2.4H_2O$, $(NH_4)_6Mo_7O_{24}.4H_2O$, $Sr(NO_3)_2$ and $Ba(NO_3)_2$ were used as the starting materials. The purity of all of these starting materials was greater than 99.99%. Appropriate amounts of the metal salts were weighed and their aqueous solutions made by dissolving the salts in deionised water. Citric acid was added as the fuel cum complexant to a homogeneous mixture of the metal-ion solutions. Ethylene glycol was used to enhance gelation and the resultant solution was dried at 333 K. The dried gel was calcined at 1173 K to completely remove the carbonaceous matter. The temperature of calcination was chosen on the basis of simultaneous Thermogravimetry (TG)/Differential thermal analysis (DTA) runs on the dried gels. The TG/DTA measurements were made using a Bähr model thermoanalyser (STA 502) at a heating rate of 10 K/min in air. The fine powder obtained after the calcination was compacted isostatically at 800 kN into cylindrical disks and finally sintered at 1473 K for 24 h in air. A flow chart for the synthesis procedure is given in Fig. 1.

2.2. Characterization

The bulk density of the sintered disks was measured by geometry as well as by mercury porosimetry. The disks were then pulverised and subjected to powder XRD as well as DTA for detecting the presence of any phase transition.

The XRD for Rietveld analysis was done using a Siemens D 5000 diffractometer with the sample (average particle size <1 μm) spread on a Si wafer in order to have a minimum interference from the background. Cu K_α was used as the incident radiation and the data were collected with a position sensitive detector over a 2θ range from 10° up to 120° with a step size of 0.008° and a counting time of 1 s per step. A whole powder pattern structure refinement using the structure analysis software TOPAS was carried out for determination of the lattice constants.

The thermal analysis runs were performed using a Setaram thermoanalyser at a heating rate of 10 K/min in purified argon atmosphere using a platinum crucible for containing the sample. The thermal analysis measurements were repeated for the cooling cycle at the same rate. It should be mentioned that all the thermal analysis data were collected on equal masses of samples so that a comparison of the intensities of the peaks could be made.

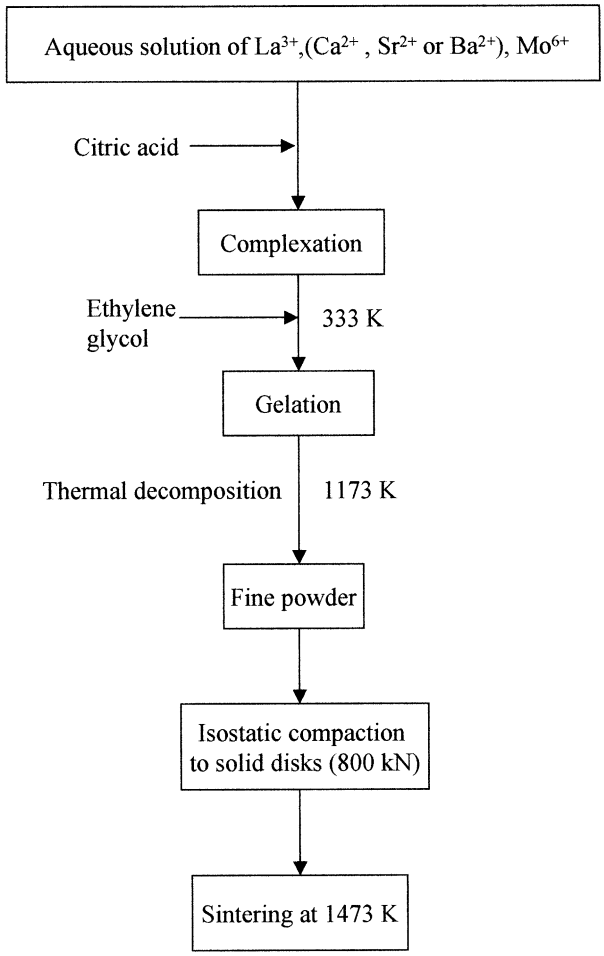

Fig. 1. Flowsheet for the synthesis of doped $La_2Mo_2O_9$.

Optical micrographs were recorded on the surface of the samples polished to a roughness of less than 1 μm. The polished surface was subjected to thermal etching (1273 K; 20 min) until the grain boundaries were clearly visible under the microscope.

Impedance spectra for some typical compositions were recorded by two probe measurements using a Solartron 1255 frequency response analyser over the frequency range from 1 MHz up to 0.1 Hz using an ac amplitude of 10 mV. The samples were painted with platinum paste on parallel surfaces and fired at a temperature of 1273 K in air for 5 min to form an oxygen reversible electrode. The data were collected for both the heating and cooling cycles.

3. Results and discussion

3.1. Synthesis

The TG/DTA plots of a typical composition, i.e. 5 mol% CaO doped $La_2Mo_2O_9$ is shown in Fig. 2. The initial loss of weight starting at ~423 K is due to

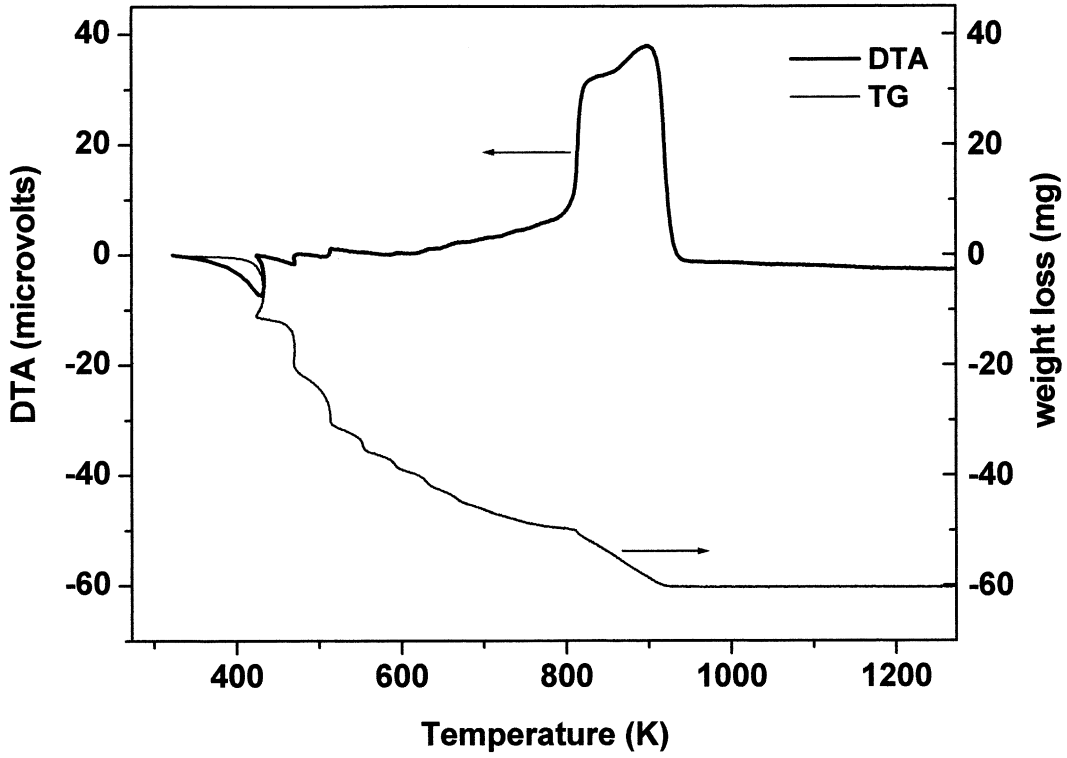

Fig. 2. TG/DTA traces for the dried gel of 5 mol% CaO doped $La_2Mo_2O_9$.

removal of the adsorbed water. The weight loss occurring thereafter is due to a stepwise burning out of the organic matter. After 923 K, there is apparently no loss of weight, which implies that all carbonaceous matter is burnt out by 923 K. Though all the samples could have been calcined at 923 K since the product formation should be complete at the temperature, they were calcined at 1173 K in order to improve the crystalline nature of the product. The XRD of the calcined samples showed a high degree of crystallinity and confirmed the formation of the product. The chemical analysis of the calcined samples indicated very low levels of C and H, i.e. <0.03 wt.%. This observation implies that the method of synthesis used in the present investigation is capable of yielding pure and highly crystalline materials at low temperatures. This is all the more worth mentioning since a negligible C impurity is a general matter of concern when wet chemical routes are employed for the synthesis of ceramics.

3.2. Characterization

The measured densities of all samples heat-treated at 1473 K (24 h) by geometry as well as mercury porosimetry were nearly 90% of the theoretical values calculated from the lattice parameters. A plot of the XRD patterns of the seven compositions of CaO doped $La_2Mo_2O_9$ is shown in Fig. 3. It is evident that there are additional peaks occurring in the patterns corresponding to 5, 10 and 15 mol% CaO doping at positions indicated by shaded circles in Fig. 3. Also, the intensities of these additional peaks are found to increase with increasing amount of CaO. The XRD patterns for compositions containing lower than or equal to 4 mol% of CaO match very well with the high temperature cubic form of $La_2Mo_2O_9$, which implies that the cubic form can be stabilized at room temperature by doping with CaO of up to 4 mol%. The lattice parameters for all compositions were refined on the basis of the structure solved by Lacorre et al for the high temperature form of $La_2Mo_2O_9$: space group P 2_13; $a=7.2014$ A°.[2] Except for the 15 mol% composition, the lattice constants for all other compositions could be refined with a low Bragg error and hence, the value for the former is not included here. A plot of the lattice constants versus the CaO content is shown in Fig. 4. Since Ca^{2+} is slightly smaller in size than La^{3+} and in addition, since substitution of a lower valent ion in the La^{3+} sites leads to creation of O^{2-} vacancies, the cell volume lowers with increasing CaO content. After 4 mol% CaO, the lattice constant is apparently invariant, which implies that any further addition leads to precipitation of a second phase. Moreover, additional peaks appear in the XRD patterns at compositions greater than 4 mol%, which clearly indicates that the limit of solubility of CaO in $La_2Mo_2O_9$ is 4 mol%. The extra peaks could be attributed to the presence of $CaMoO_4$ which is indicated in Fig. 3. The pattern for the undoped $La_2Mo_2O_9$ is not included in Fig. 4 as all the patterns were recorded at room temperature. The room temperature crystal

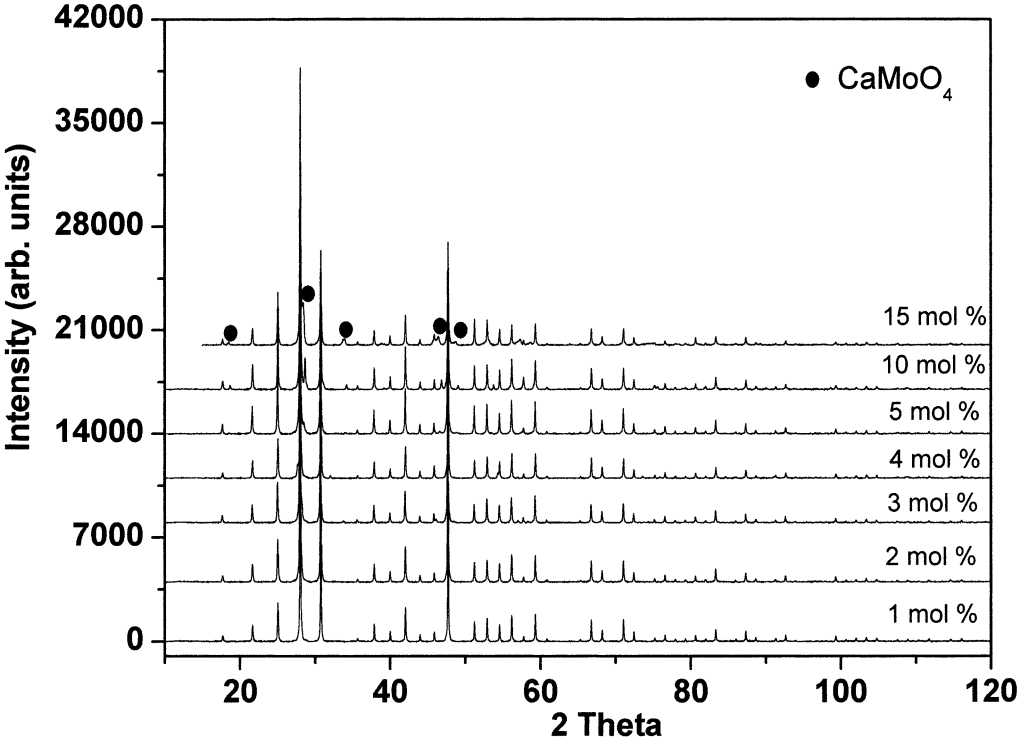

Fig. 3. XRD patterns of $(La_{1-x}Ca_x)_2Mo_2O_{9-\delta}$; $0.01 \leqslant x \leqslant 0.15$.

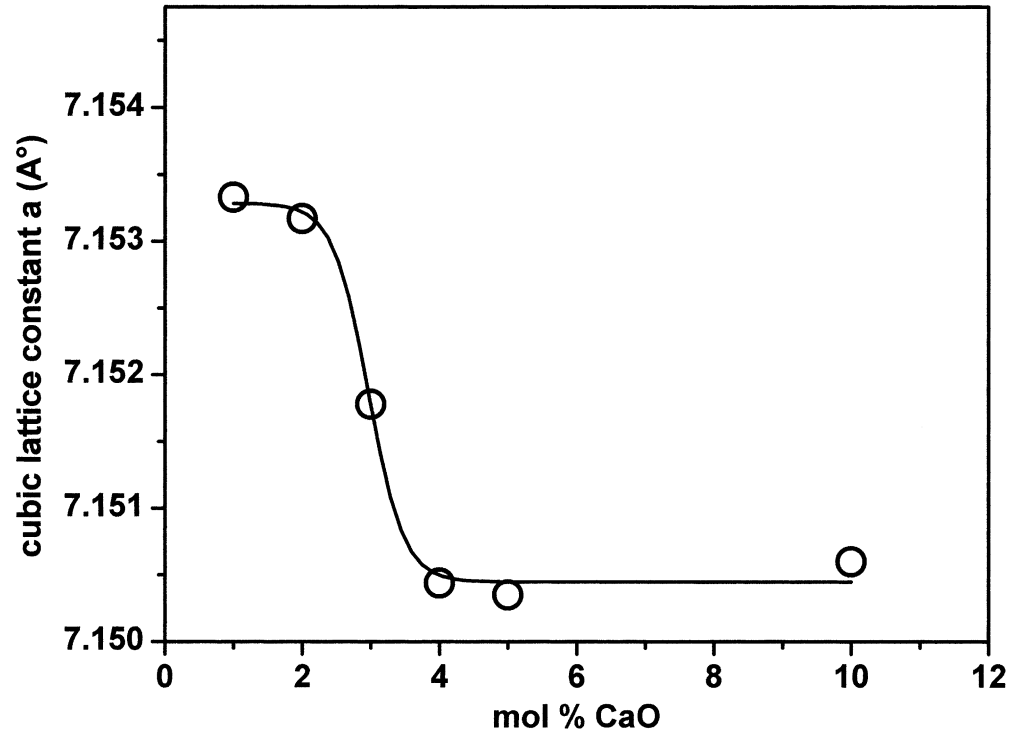

Fig. 4. Cubic lattice constant as a function of different amounts of CaO doping.

structure of $La_2Mo_2O_9$ is not cubic as can be seen from Fig. 5. A careful observation of the XRD patterns depicted in Fig. 5 shows that the diffractogram for the undoped sample exhibits a peak splitting at 2θ 43–45 °, 68–70° and after 80°, which give clear evidence that the low temperature form is of a lower symmetry and thus not cubic. A similar procedure was adopted for the determination of the cubic lattice constants of SrO and BaO doped $La_2Mo_2O_9$. A comparison of the XRD patterns of the alkaline-earth doped $La_2Mo_2O_9$ with that of

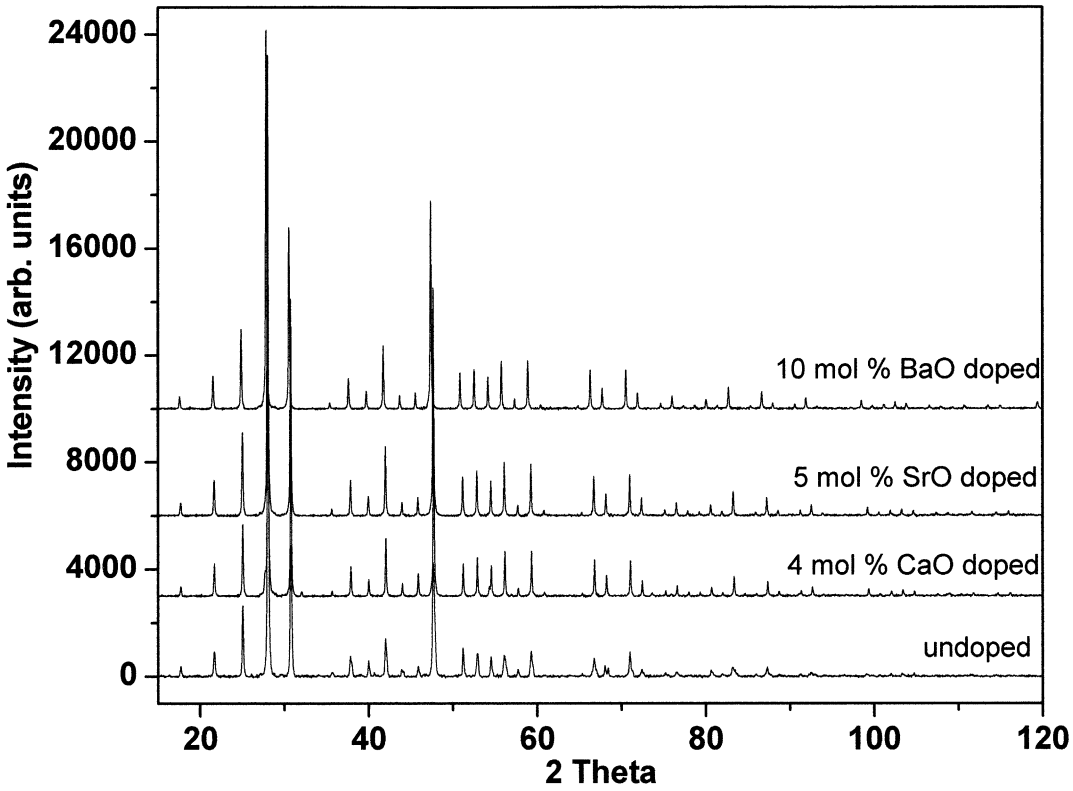

Fig. 5. XRD patterns of $(La_{1-x}M_x)_2Mo_2O_{9-\delta}$; $M = Ca^{2+}$, Sr^{2+} and Ba^{2+}.

undoped $La_2Mo_2O_9$ obtained in the present study is shown in Fig. 5. Table 1 gives the calculated lattice constants for all samples investigated in this study along with their respective Bragg errors after refinement. The index for the matching of the calculated pattern with the measured one for the whole 2θ range, increases from 4 mol% CaO up to 15 mol%. This is in accordance with the expectation. Fig. 6 shows the cubic lattice constant as a function of the ionic radius in the case of the alkaline-earth doped $La_2Mo_2O_9$. The lattice parameter increases significantly with the ionic radius as expected from the increase of the ionic radius ($r_{Sr2+} = 131$ pm and $r_{Ba2+} = 147$ pm for nine-fold coordination).[7] Since Sr^{2+} and Ba^{2+} are also aliovalent dopant ions like Ca^{2+}, substitution by these ions in La^{3+} sites also leads to formation of oxygen vacancies. But as both Sr^{2+} and Ba^{2+} are larger than La^{3+}, they partially occupy also the space created by the neighbouring oxygen vacancies and still stabilize the structure. Ba^{2+} being the largest when compared with Sr^{2+} and Ca^{2+}, is able to effectively extend its occupation to the nearest oxygen vacancy site and hence, the solubility limit increases in the order $Ba^{2+} > Sr^{2+} > Ca^{2+}$. This is the reason why the solubility limits of SrO and BaO in $La_2Mo_2O_9$ are higher than that of CaO.

The verification of the suppression of the phase transition by aliovalent substitution was carried out by thermal analysis. The results are presented in Figs. 7 and 8. Since all thermal analysis runs were performed with equal masses of samples, the intensities of the peaks can be compared with each other. It is seen from Fig. 7 that only the 4 mol% composition shows a flat

Table 1
Lattice constants obtained by Rietveld refinement for various dopant concentrations of CaO compared with that for 5 and 10 mol% doping of SrO and BaO in $La_2Mo_2O_9$

Dopant	Composition (mol%)	Cubic lattice constant (A°)	Error (A°)	R_{Bragg}	R_{wp}
CaO	1	7.15331	0.00003	5.490	5.625
CaO	2	7.15317	0.00006	5.568	5.884
CaO	3	7.15178	0.00006	7.024	5.884
CaO	4	7.15044	0.00006	7.299	5.906
CaO	5	7.15035	0.00006	6.374	6.010
CaO	10	7.15060	0.00008	6.019	7.826
SrO	5	7.15822	0.00005	5.408	5.908
BaO	10	7.19637	0.00006	5.336	5.848

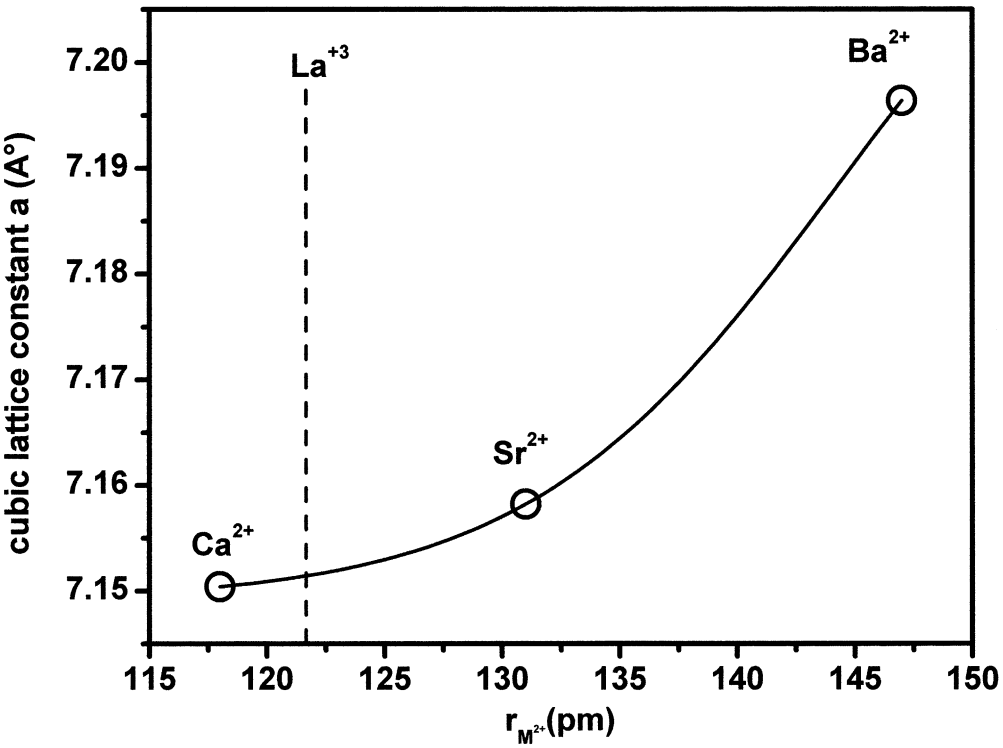

Fig. 6. Cubic lattice constant of alkaline-earth doped $La_2Mo_2O_9$ as a function of ionic radius of the dopant.

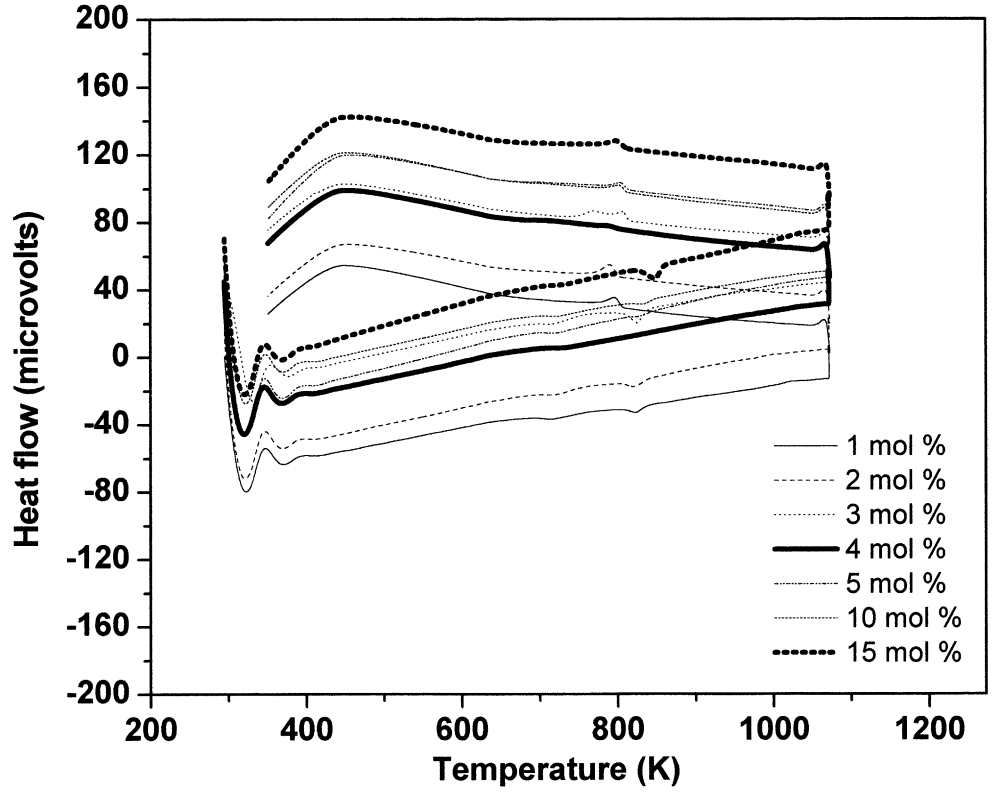

Fig. 7. DTA traces of $(La_{1-x}Ca_x)_2Mo_2O_{9-\delta}$; $0.01 \leqslant x \leqslant 0.15$.

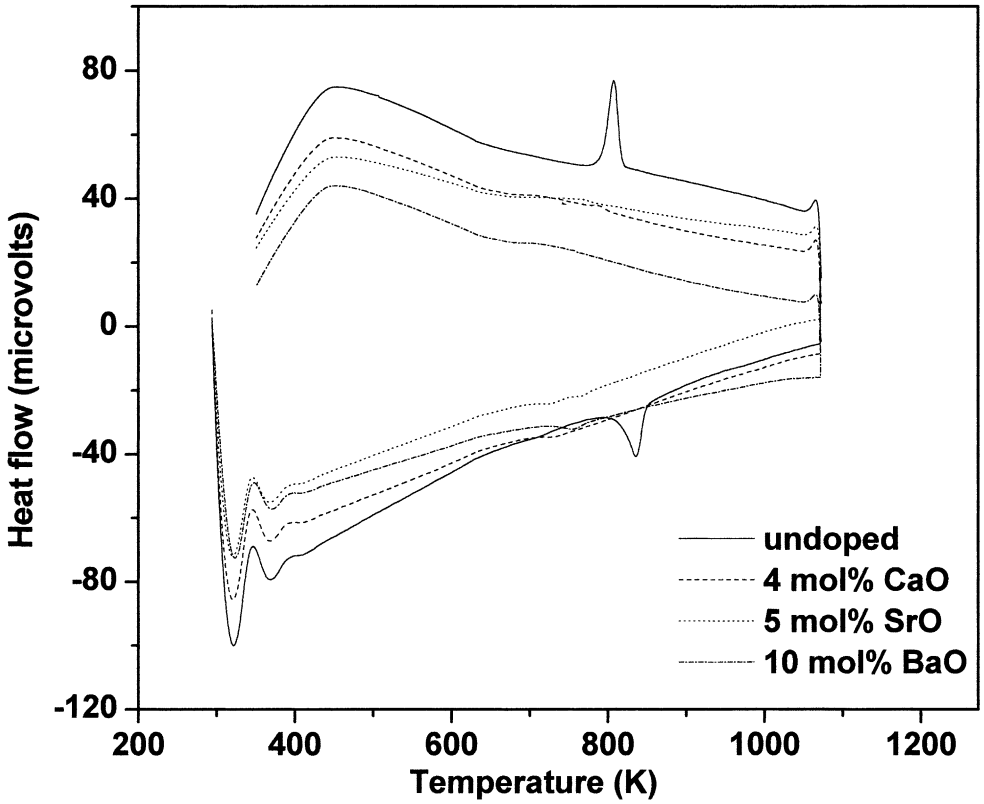

Fig. 8. DTA traces of $(La_{1-x}M_x)_2Mo_2O_{9-\delta}$; Ca^{2+}, Sr^{2+} and Ba^{2+}.

curve, whereas the traces for the rest of the compositions show an endothermic peak on heating (between 803 and 853 K) and an exotherm on cooling, which is a characteristic of first order reversible phase transition. This clearly indicates that only the 4 mol% doping is able to completely mask the phase transition in $La_2Mo_2O_9$. A comparison of the DTA traces of Ca^{2+}, Sr^{2+} and the Ba^{2+} doped $La_2Mo_2O_9$ bearing the composition of the solubility limit is made in Fig. 8. All traces show a suppressed phase transition peak, which implies that these compositions are capable of fully stabilizing the high temperature phase at room temperature.

The impedance spectra of the compositions under investigation showed two semicircles. The spectra obtained at 773 K for all compositions are compiled in Fig. 9. Only a part of the first semi-circle is shown for the sake of clarity. The intersection of the beginning of the first semicircle with the x-axis was considered as the resistance due to the bulk of the sample. The impact of the leads was corrected from the measured bulk resistance and the electrical conductivity evaluated from appropriate blank measurements. A plot of the electrical conductivities as a function of the inverse temperature is shown in Fig. 10. The SrO doped $La_2Mo_2O_9$ exhibits the maximum conductivity. It was also found that in case of the BaO doped sample, measurements in flowing air and pure oxygen yielded the same values of the conductivity which means that in these ranges of oxygen partial pressures, the conductivity is predominantly ionic in nature, though the conductivity values were lower than that of the 15 mol% CaO doped sample. This invariance in the conductivity over the p_{O_2} range from pure O_2 (101.3 kPa) up to air (21.1 kPa) could be expected for all the doped samples. In addition, all samples except the 4 mol% CaO doped one, show a slight bending at around 830–900 K. This may be due to the structural phase transition occurring in the samples, which does not occur in the sample of 4 mol% CaO doping. This observation again confirms that a 4 mol% doping of $La_2Mo_2O_9$ with CaO completely suppresses the transition. The electrical conductivities however do not exhibit any specific trend with different amounts of CaO doping.

From the optical micrographs, the average grain size for all samples was determined to range from 5 to 15 μm. The total porosity was found to be less than 10%. During the process of etching, when the samples were quenched rapidly from 1273 K to room temperature, they cracked. This observation could lead to the conclusion that the thermal shock resistance of the material may not be attractive for technological applications. The use of suitable additives may improve this property.

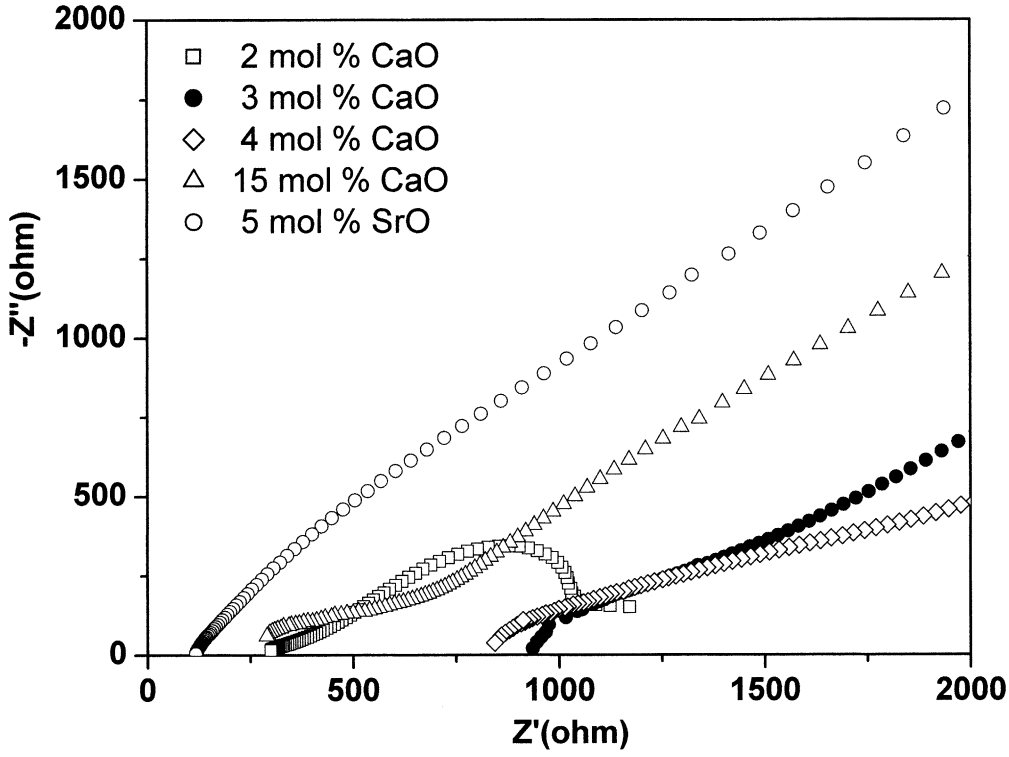

Fig. 9. Comparison of the impedance spectra of $(La_{1-x}Ca_x)_2Mo_2O_{9-\delta}$; $0.02 \leqslant x \leqslant 0.15$ with $(La_{0.95}Sr_{0.05})_2Mo_2O_{9-\delta}$ at 773 K.

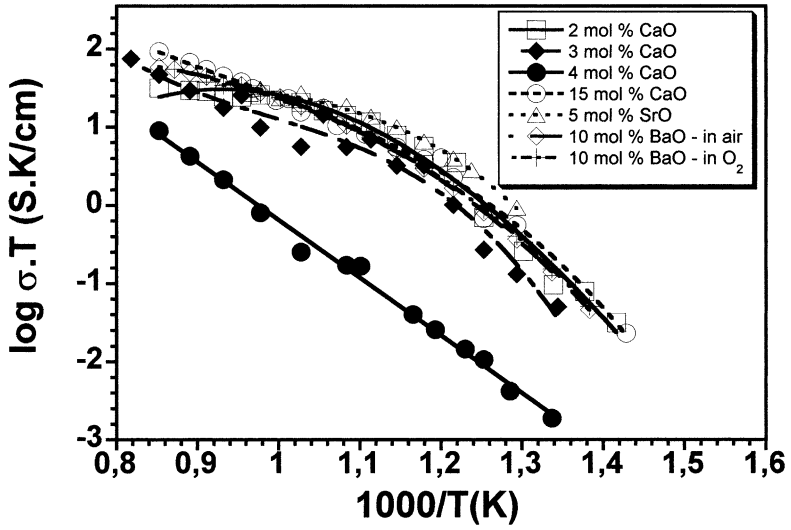

Fig. 10. Plot comparing the electrical conductivities of $(La_{1-x}Ca_x)_2Mo_2O_{9-\delta}$; $0.02 \leqslant x \leqslant 0.15$ with $(La_{0.95}Sr_{0.05})_2Mo_2O_{9-\delta}$ and $(La_{0.90}Ba_{0.10})_2Mo_2O_{9-\delta}$.

4. Conclusion

The results of the present investigation indicate that not more than 4 mol% of CaO can be incorporated on the La^{3+} sites of $La_2Mo_2O_9$. Any further addition of CaO results in the formation of a second phase, i.e. $CaMoO_4$. With respect to the other alkaline-earth dopants, Sr^{2+} and Ba^{2+}, the solubility limits reported by Lacorre et al. were verified.

Acknowledgements

The authors would like to thank Mr. U. Klock (Max-Planck-Institut für Festkörperforschung, Stuttgart, Germany) for the thermal analysis measurements. One of the authors, R. Subasri, would like to acknowledge the Max-Planck-Society for the financial support provided in the form of a fellowship.

References

1. Lacorre, Ph., Goutenoire, F., Bohnke, O., Letoux, R. and Laligant, Y., Designing fast oxide-ion conductors based on $La_2Mo_2O_9$. *Nature*, 2000, **404**, 856–858.
2. Goutenoire, F., Isnard, O., Retoux, R. and Lacorre, Ph., Crystal structure of $La_2Mo_2O_9$, a new fast oxide-ion conductor. *Chem. Mater*., 2000, **12**, 2575–2580.
3. Lacorre, Ph., The LPS concept, a new way to look at anionic conductors. *Solid State Sciences*, 2000, **2**, 755–758.
4. Fournier, J. P., Fournier, J. and Kohlmuller, R., Ètude des systémes La_2O_3–MoO_3, Y_2O_3–MoO_3 et des phases Ln_6MoO_{12}. *Bull. Soc. Chim. Fr*, 1970, 4277.
5. Goutenoire, F., Isnard, O., Suard, E., Bohnke, O., Laligant, Y., Retoux, R. and Lacorre, Ph., Structural and transport characteristics of the LAMOX family of fast oxide-ion conductors, based on lanthanum molybdenum oxide $La_2Mo_2O_9$. *J. Mater. Chem*., 2000, **11**, 119–124.
6. Wang, X. P. and Fang, Q. F., Effects of Ca doping on the oxygen ion diffusion and phase transition in oxide ion conductor $La_2Mo_2O_9$. *Solid State Ionics*, 2002, **146**, 185–193.
7. Shannon, R. D., Revised effective ionic radii and systematic studies of interatomic distances in halides of chalcogenides. *Acta Crystallogr*., 1969, **A32**, 751–767.